Available online at www.sciencedirect.com

ScienceDirect

journal homepage: www.elsevier.com/locate/he

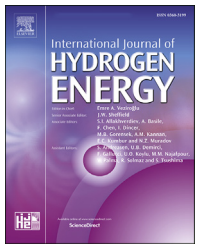

An alternative route to produce easily activated nanocrystalline TiFe powder

R.B. Falcão [a], Edgar D.C.C. Dammann [a], C.J. Rocha [a], M. Durazzo [b], R.U. Ichikawa [a], L.G. Martinez [a], W.J. Botta [c], R.M. Leal Neto [a,*]

[a] Material Science and Technology Center, Nuclear and Energy Research Institute- IPEN-CNEN/SP, Av. Prof. Lineu Prestes, 2242, CEP 05508-000, São Paulo, SP, Brazil

[b] Nuclear Fuel Center, Nuclear and Energy Research Institute - IPEN-CNEN/SP, Av. Prof. Lineu Prestes, 2242, CEP 05508-000, São Paulo, SP, Brazil

[c] Materials Engineering Department, Federal University of São Carlos, Rod. Washington Luiz, Km 235, CEP 13565-905, São Carlos, SP, Brazil

ARTICLE INFO

Article history:
Received 18 March 2018
Received in revised form
15 June 2018
Accepted 6 July 2018
Available online 26 July 2018

Keywords:
TiFe
Hydrides
Ball milling
Hydrogen storage
Mechanical activation

ABSTRACT

In this paper, an alternative process route to produce active nanocrystalline TiFe compound was investigated. First, TiH_2 and Fe powders were dry co-milled in a planetary ball mill for 5–40 h. TiH_2 was selected as precursor powder, instead of Ti powder, due its fragility, which has proved to be beneficial to decrease powders adherence on milling tools. In terms of loose powder mass, milling yields ranged from 90 to 95 wt.%. Next, milled powders were post-heated at 873 K under dynamic high-vacuum for TiFe synthesis reaction. First hydrogen absorption was verified *in situ* during the cooling process of samples (until the room temperature), being the amount of hydrogen absorbed and desorbed by this samples measured by automated Sievert's apparatus, under constant hydrogen flow rate of 9 cm^3. min^{-1} (dynamic measurements). Besides to allowing the first absorption *in situ*, the investigated process route also allowed the production of the non-stoichiometric TiFe compound (rich in Ti) in samples milled for shorter times (5 and 10 h), both characteristics associated with maintaining the mechanical compound activity. Each sample absorbed hydrogen at 2 MPa during the cooling process, requiring no additional thermal activation cycles, since the samples milled for shorter times (mainly for 10 h) could absorb hydrogen for the first time more easily. However, the samples milled for longer times (25 and 40 h) shown better results in terms of reversible and storage capacities (0.73 and 0.94 wt.%, respectively).

Introduction

It's known that TiFe intermetallic compound can storage large amounts of hydrogen at room temperature and at relative low pressures (about 1.9 wt.% of H_2 at room temperature) [1,2]. Despite its high volumetric hydrogen density (about 115 kgH_2. m^{-3} for $TiFeH_{1.7}$) [3], the high density of the TiFe hydrides (>5.5 g. cm^{-3}) have directed its use to stationary [4,5] or naval

* Corresponding author.
E-mail address: lealneto@ipen.br (R.M. Leal Neto).

https://doi.org/10.1016/j.ijhydene.2018.07.027

[6] applications. A very known difficulty of this AB compound is that an activation procedure is commonly necessary to the first hydrogen absorption, especially when it is produced by melting (induction or arc furnaces). Usually, this activation procedure consists of slow and complicated heat treatment cycles, alternating heating at high temperatures with cooling, and high hydrogen pressure with high vacuum levels [1,7–10].

In attempt to overcome this problem and to improve hydrogenation properties, several approaches have been carried out. One of them is to change the chemical composition, adding other elements, like Al [11], B, C, Co [11,12], Cr [13], Cu [10], Mn [5,13,14], Nb [15–17], Ni [11,14,18], Pd [19,20], V [5,21], Zr [16,22–24] and Y [25]. Generally, these alloying elements cause an improvement on activation and kinetics, but with a reduction in the hydrogen capacity. With the same purpose in mind, alternative processing routes have been investigated to produce TiFe as well. Among them we can highlight the high-energy ball milling, either from Ti and Fe elementary powders (mechanical alloying) [26–34], or from TiFe powder previously obtained by melting and then grinding or ball milling (mechanical milling) [14,26,31,35–39].

In fact, several authors reported that TiFe compound was already active after the milling process, requiring no post activation procedures to absorb hydrogen at room temperature [28,30,31,35,37,39]. From a review of articles since the 1990s, two main groups can be considered regarding where the first hydrogen absorption took place: *in situ* reaction group, e.g., absorption occurred in the same place (in this case, the milling vial) where TiFe compound was produced [28,35,37]; *ex situ* group, in which milled powder is transferred from the vial to a Sievert's apparatus, where first absorption occurred [30,31,39].

It has also been reported that TiFe didn't remain active after milling, still requiring thermal activation cycles at hydrogen pressure alternated with vacuum for first absorption [26,29,40]. Zadorozhnyy *et al.* [40], for example, had to reactivate milled material (for 2 h with 840 rpm) using degassing cycles under vacuum followed by heating with hydrogen at 1 MPa and 673 K. The deactivation of milled compound is well-known in literature, being almost always related to superficial poisoning of powder particles, especially by oxygen, either during the milling process, or even in the transportation to an external reactor of the Sievert's apparatus [26,41]. However, what keeps TiFe activity after milling, even when exposed to oxygen, has been less explored in literature [30,31,39]. In spite of that, there are strong evidences that activity maintenance can be associated with compositional variation of TiFe compound (Ti-rich compound) [42,43]. Therefore, regarding to the maintenance of TiFe activity after milling, we have distinct explanations on each inferred group: lower exposure to oxygen (*in situ* reactions) [28,35,37]; higher superficial resistance to oxygen due to compositional variation of TiFe compound (*ex situ* reactions) [30,31,39].

Besides keeping TiFe activity after milling process, it's also important control the strong adherence, either from Ti and Fe elementary powders, or from TiFe powder, on the milling tools (mainly on the vial), thus ensuring a higher yields to process (in terms of loose powder mass) [30,39,44]. Abe *et al.* [30], for example, observed yield losses up to 40% after milling for 40 h. Commonly, this adherence is controlled by addition of organic PCAs (Process Control Agents), like ethanol, stearic acid, low density polyethylene, benzene, cyclohexane and acetone. However, it was verified that many of these organic PCAs can be decomposed during the milling process, thus contaminating the milled material [39,45]. An alternative to avoid these problems may be substitute TiH_2 for Ti. TiH_2 is fragile, which is benefic to decrease powders adherence on milling tools, and has no strange chemical elements to the system Ti–Fe–H as well [45].

In view of the foregoing considerations, this work deals with an alternative process route based on ball milling and external *in situ* reaction combining a low yield loss by adherence and a stable milled material ready to produce an active TiFe. To achieve these goals, TiH_2 and Fe powders were high-energy ball milled, followed by a post-heating treatment under vacuum to provide the reaction synthesis of the desired compound in the Sievert's apparatus, where hydrogenation will take place (external *in situ* reaction).

Materials and methods

Ti and Fe powders (99.7 and 99.9% of purity, −325#) were supplied by AEE® (Atlantic Equipment Engineers). Initially titanium hydride (TiH_2) was produced by heating Ti powder under 10 bar hydrogen atmosphere up to 773 K. TiH_2 and Fe powders were then weighted according to the TiFe compound stoichiometry (50:50). A planetary mill (Pulverisette 5 from FRITSCH®) was used to perform mechanical alloying. Each milling charge consisted of 295 balls, made of tool steel ($\varnothing = 8$ mm), and 30 g of TiH_2 and Fe powders mixture, equivalent to a ball-to-powder weight ratio of 20:1. A cylindrical rounded-bottom vial, made of hardened steel ($V = 250$ cm^3), was used for planetary milling, always operated at 300 rpm. Powders were handled in glove box with purified argon atmosphere during charge and discharge operations. Samples were dry milled for 5, 10, 25 and 40 h.

X-ray diffraction (XRD) from Cu-Kα radiation, scanning electron microscopy with energy-dispersive X-ray spectroscopy (SEM-EDX), differential scanning calorimetry associated to thermogravimetric analysis (DSC-TG) and transmission electron microscopy (TEM) were used for characterizing microstructure and phase transformations of the as-milled and heat-treated powders. DSC-TG was performed with a heating rate of 10 K. min^{-1} up to 1273 K under a constant argon flow (10^3 cm^3. h^{-1}). XRD patterns of the samples were analyzed by the Rietveld refinement method using the Diffrac^{Plus} TOPAS 4.2 from BRUCKER®. Modified "Thompson-Cox-Hastings pseudo-Voight" profile shape function was employed for mean crystallite size ($<L>_v$) and microstrain (ε) calculations, in which the peak profile is considered to be a convolution of Gaussian and Lorentzian functions [46]. Solubility degree of the alpha iron phase in the as-milled material was estimated assuming a linear variation of lattice parameter and using the data from Abrahamson & Lopata [47].

As-milled powders, about 2 g, were heat-treated at 873 K under vacuum, in a reactor of the automated Sievert's apparatus (own design and construction), for TiFe synthesis reaction. Immediately after reaction, the reactor was pressurized with hydrogen at 2 MPa (99.999% purity), being the first

Table 1 – Yields (Y) and chemical composition of the as-milled powders for different times.

Milling time [h]	Y [wt.%]	Area analysis[a] at.% (σ)		Point analysis[b] at.%		
		Ti	Fe	Ti	Fe	Cr
5	92	52.7 (4)	47.3 (4)	10.4	89.6	–
10	90	52.11 (4)	47.89 (4)	16.5	83.5	–
25	93	50.94 (16)	49.06 (16)	19.82	79.54	0.64
40	95	50.93 (15)	49.07 (15)	8.32	90.95	0.73

[a] Area analysis refers to the mean of three areas (about 100 μm^2) over random particles with the respective standard deviation.
[b] Point analysis over random visible Fe-rich regions.

hydrogen absorption verified during the material cooling process (at same cooling rate). The sorption properties of the reacted compound were measured in the same Sievert's apparatus operating in dynamic mode under a hydrogen constant flow (9 cm^3. min^{-1}). Trapped hydrogen in reacted samples after hydrogenation was estimated by inert gas fusion-infrared absorptiometry.

Results and discussion

TiH_2 and Fe powders milling

TiH_2 apparently acted as a non-organic PCA, avoiding the strong adherence on milling tools, behavior that can be confirmed by the resultant high yields in all as-milled samples (≥90% in terms of loose powder mass, Table 1).

In addition, TiH_2 contributed to formation of Ti-rich regions in the microstructure of the as-milled samples for shorter times (5 and 10 h), as shown in Fig. 1 (up to 5% over the initial composition of Ti, Table 1). These chemical heterogeneities are typical of *ductile-brittle* systems [48,49], like Fe–TiH_2, and tend to disappear with the increase of the milling time (25 and 40 h), producing a homogeneous mixture with chemical composition close to the TiFe stoichiometry, as also shown in Fig. 1. Fe-rich regions were observed in the microstructure of all as-milled samples. However, these regions appear to have distinct origins depending on the milling time. For shorter times (5 and 10 h), for example, Fe-rich regions appear to be derived from the low dispersion of Ti and Fe powders (Fig. 1a and b). As for longer times, these regions

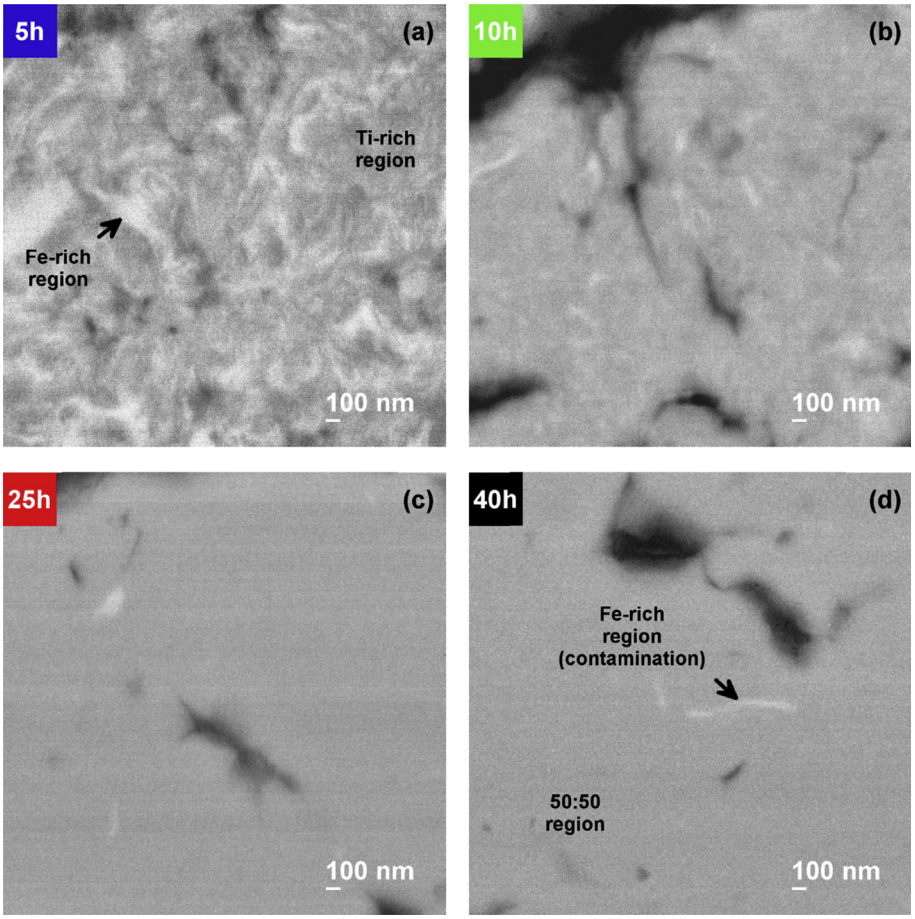

Fig. 1 – SEM images (back-scattered electrons) of the as-milled TiH_2+Fe powders after different milling times: (a) 5 h; (b) 10 h; (c) 25 h; (d) 40 h.

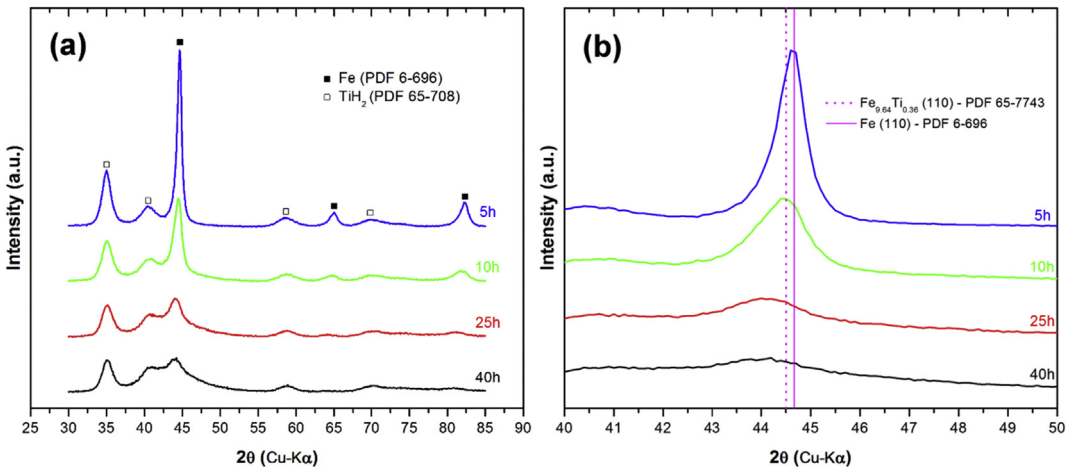

Fig. 2 – (a) XRD patterns of the as-milled powders for different times; (b) Close view on (110) peak of Fe phase in relation to (110) peak of $Fe_{9.64}Ti_{0.36}$ phase.

appear to be derived from milling tool wear (Fig. 1d), since an increase of chromium contamination was verified, as shown in Table 1 (up to 0.7 at.% for 40 h).

In spite of the reported homogeneity, the formation of TiFe compound was not detected in any as-milled powder samples, whose XRD patterns only show reflection peaks corresponding to TiH_2 and Fe phases (Fig. 2a). The decreasing of peak intensities is due to the crystalline defects produced by impacts of the balls during the milling process.

Such results indicate that the formation of TiFe, at least in process route investigated, still depends on the heat treatments. In XRD patterns yet, a systematic shift (to left) of the (110) peak from Fe phase was observed with the increasing of the milling time (Fig. 2b).

This shift can be mainly attributed to the solution of some Ti in Fe, since the Ti has a higher atomic radius than Fe. Ti content in the solid solution can be calculated by assuming a linear variation of the unit cell dimension (lattice parameter) with the solid solution composition. As a reference for the proportionality we used the data from Abrahamson & Lopata [47], in which peak shift of 0.17814° on (110) reflection is related to the solid solution Fe (Ti) with 3.6 at.% Ti. Ti content dissolved in Fe was then calculated using proportionality and the actual shift of the peak (110), measured on each sample pattern. The variation of the Ti content in the solid solution with milling time is shown on Fig. 3. Free Ti could be originated from TiH_2 decomposition ($TiH_2 \rightarrow Ti + H_2$) during the milling process.

TiFe synthesis reaction

DSC-TG analysis was initially performed on as-milled samples in order to investigate how the reaction occurred. In DSC curves (Fig. 4a), two endothermic peaks can be seen, at 500 K and 700 K, both attributed to the decomposition of TiH_2 ($TiH_2 \rightarrow Ti + H_2$), which can be related to the mass loos shown in every TG curve (Fig. 4b). The decreasing mass loss is due to some previous decomposition of TiH_2 during the milling process, corroborating with Ti solubility increase (Fig. 3) denoted by the XRD peak shift shown before.

In DSC curves yet, two exothermic peaks, at 773 K and 1010 K, can be seen. Fist peak was attributed to the TiFe reaction synthesis, confirmed by XRD analyzes after heat treatments at 873 K (Fig. 5a). The second peak can be related to the Fe_2Ti formation trough oxidation of TiFe (possibly $Ti_{3.9}Fe_{2.1}O \rightarrow Ti_3Fe_3O + TiO_{0.325}$), result that could be confirmed by the increasing amount of these phases (Table 2) after heat treatments at 1073 K (Fig. 5c). Such results indicated that heat treatments should be performed at temperatures ranging from 750 to 873 K, thus avoiding significant oxidation of TiFe.

After determining the heat treatment temperature range for the TiFe synthesis reaction, as-milled samples were heated at 873 K under vacuum, in a reactor of the Sievert's apparatus. TiFe phase was mostly formed (≥98 wt.%, Table 2) from samples milled for longer times (25 and 40 h), as shown in XRD patters (Fig. 5a). However, in samples milled for shorter times (5 and 10 h), some Fe (up to 16 wt.%, Table 2) and Ti-oxide (possibly $TiO_{0.325}$ up to 3 wt.%, Table 2) were observed. Ti

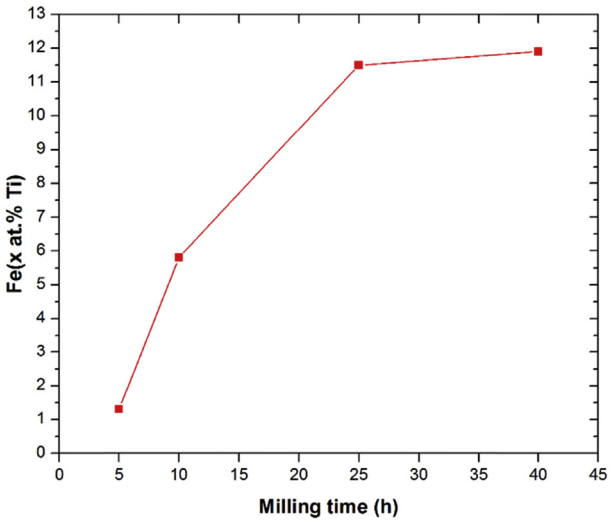

Fig. 3 – Variation of the Ti content (x at.% Ti) dissolved in Fe with milling time.

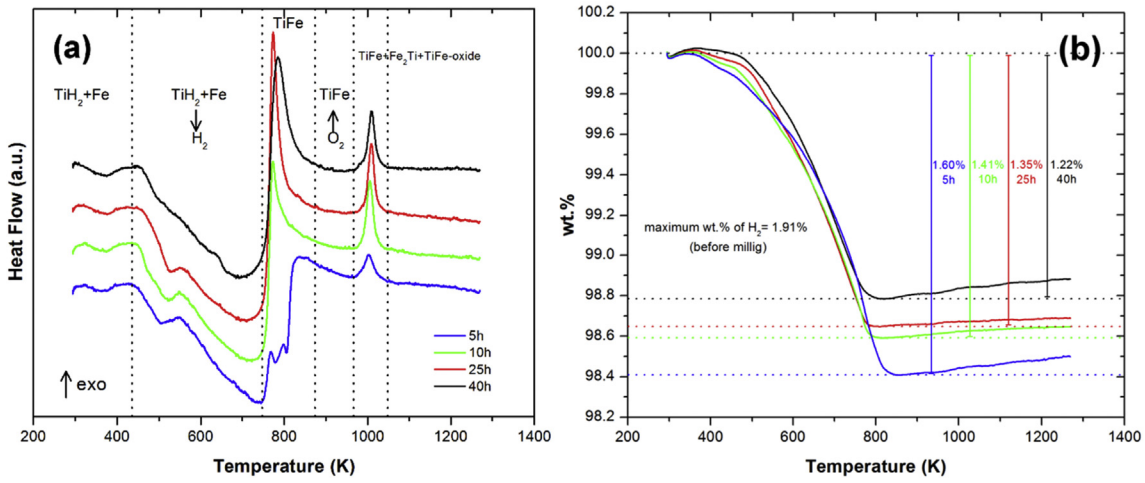

Fig. 4 – (a) DSC and (b) TG curves of TiH_2+Fe mixture with milling time.

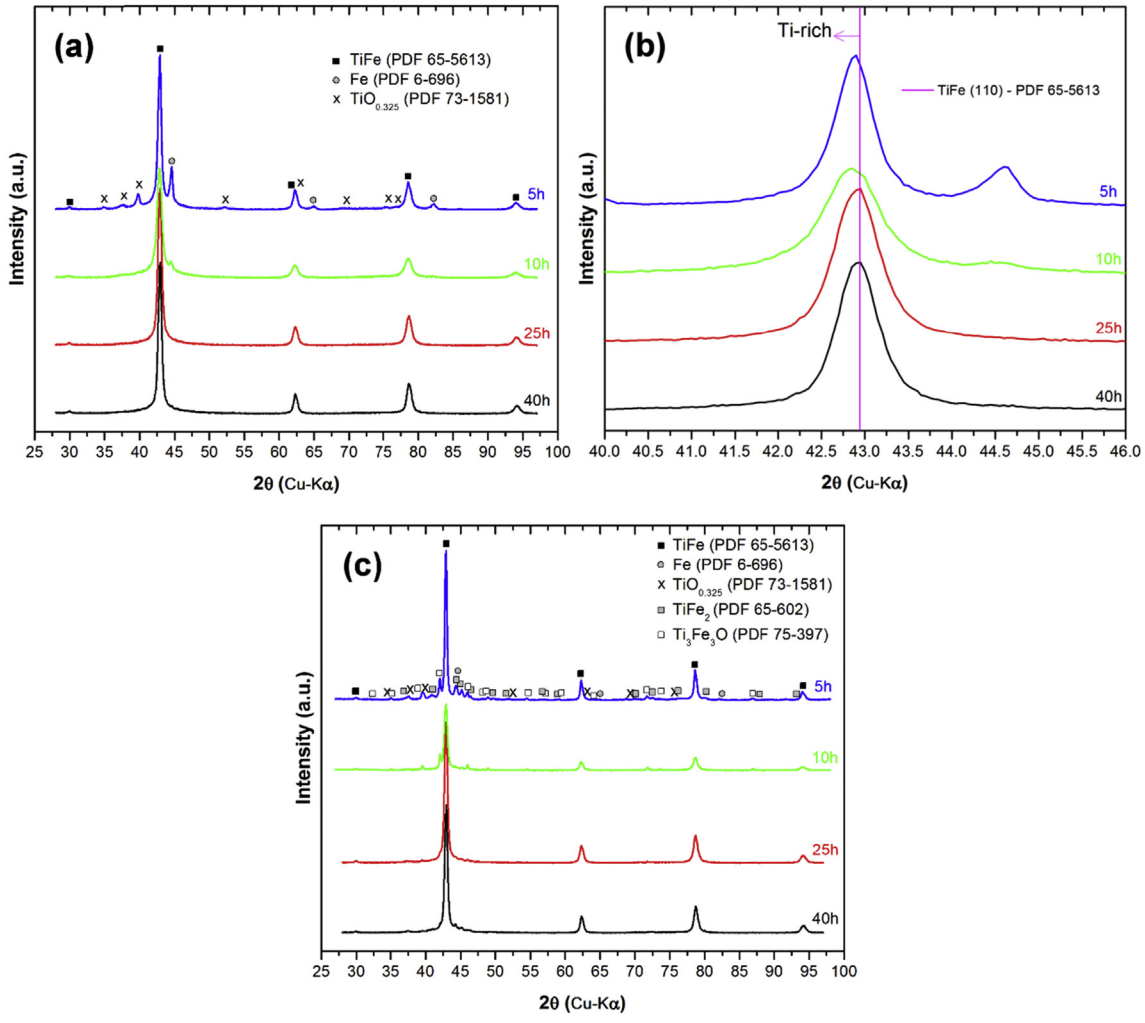

Fig. 5 – (a) XRD patterns of reacted samples at 873 K (milling times indicated); (b) Close view on (100) peak of TiFe phase; (c) XRD patterns of reacted samples at 1073 K (milling times indicated).

oxidation was probably occurred during the heat treatments. In these samples (milled for 5 and 10 h), as already observed in Fig. 1, the resultant heterogeneous powder mixtures impaired the complete reaction synthesis of TiFe, which justifies the higher amounts of free Fe and Ti-oxide ($TiO_{0.325}$).

In XRD patterns yet (Fig. 5b), a systematic shift (to left) of the (110) peak from TiFe phase was observed, mainly from samples milled for shorter times (5 and 10 h). This shift is attributed to the higher amount of non-stoichiometric TiFe phase (with higher Ti content), which should imply in a lattice expansion of TiFe (up to 0.2% over the stoichiometry TiFe pattern, Fig. 6). This shift can be related to the chemical heterogeneities previously observed (Fig. 1) and is accompanied by a microstrain increase (Fig. 7). Furthermore, this shift appears to be reduced with the increase of the milling time, which can be confirmed by the variation of TiFe lattice parameter shown in Fig. 6.

As for the crystallite size of TiFe, as shown in Fig. 7, nanostructured TiFe was always formed (crystallite size ranging from 13 to 21 nm), which is compatible with TEM analysis results (crystallites up to 10 nm, Fig. 8). Further, the mean crystallite size appears to be reduced as milling time increased, reaching a minimum value already after 10 h of milling (about 13 nm), which remained practically unchanged for longer milling times (about 14 nm for 25 and 40 h). All verified results suggest that the milling route performed could produce TiFe compound with suitable properties for first hydrogen absorption.

First hydrogen absorption

Once established the processing route to produce TiFe, reacted samples (at 873 K) were immediately pressurized with hydrogen at 2 MPa (in the same reactor where TiFe was produced). The first hydrogen absorption was verified in all samples during the cooling process (until the room temperature), requiring no post activation procedure, as shown in Fig. 9 by the relative hydrogen absorption (relative to maximum hydrogen absorption of the sample milled for 40 h). Such results confirmed that TiFe was remained active on the investigated route. Though, the hydrogen absorption (dissociation and penetration) appears to be facilitated in samples milled for shorter times (mainly for 10 h), which absorbed hydrogen at higher temperatures, before the others (Fig. 8), result that was attributed to a higher compositional variation of TiFe (rich in Ti).

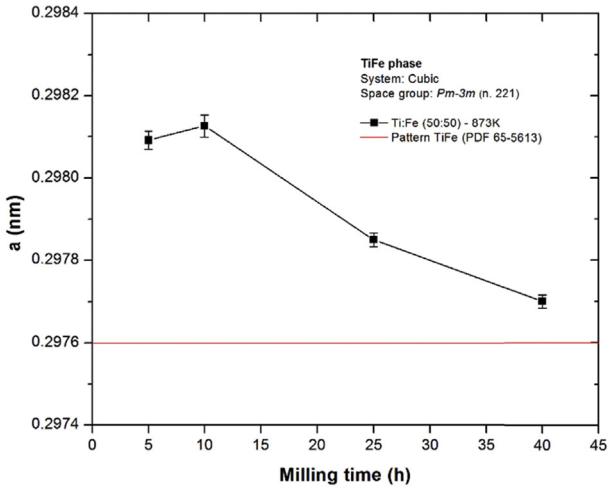

Fig. 6 – Variation of TiFe lattice parameter for different milling times.

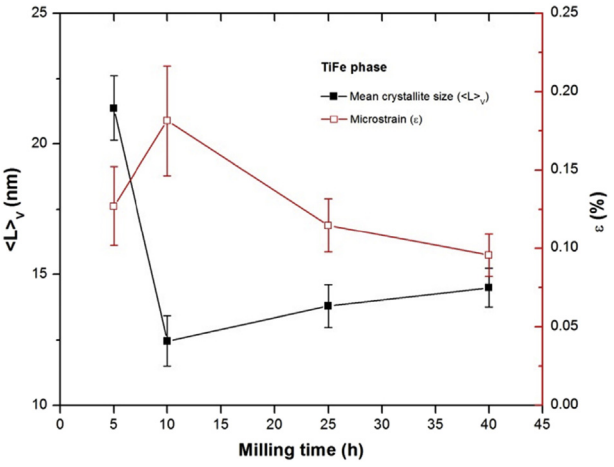

Fig. 7 – Mean crystallite size and microstrain of TiFe for different milling times.

Concerning to related phenomenon, Ti-rich samples also should exhibit superior results in absorption kinetics (when at same initial pressure and cooling rate). In fact, 10 h milled sample shown these expected improvements on absorption kinetics, which can be confirmed by sharp drop in absorption

Table 2 – Phase composition of as-milled powders for various times after heat treatments at 873 K and 1073 K.

Milling time [h]	Heat treatment temperature [K]	Phase (wt.%)				
		TiFe	Fe	Ti-oxide ($TiO_{0.325}$)	Fe_2Ti	TiFe-oxide (Fe_3Ti_3O)
5	873	80.39	16.42	3.19	–	–
10		94.80	4.98	0.22	–	–
25		98.11	1.89	–	–	–
40		98.55	1.45	–	–	–
5	1073	68.14	9.39	1.42	6.59	14.46
10		78.14	5.64	0.07	1.81	14.35
25		90.67	4.66	0.13	2.30	2.22
40		90.22	4.65	0.06	2.90	2.17

curves from Fig. 9. However, the same shape was not observed in 5 h milled sample, which also shown a higher compositional variation of TiFe. In this case, a larger mean crystallite size would have limited the absorption kinetics. The lower content of TiFe phase in this sample (about 80 wt.%, see Table 2) may also have contributed to poor results in absorption kinetics.

Hydrogen sorption isotherms

After cooling the hydrogenated samples to the room temperature, hydrogen sorption pressure measurements were performed in the same reactor of the Sievert's apparatus. Calculated isotherms (at room temperature) are shown in Fig. 10. Lowest absorption and desorption plateaus (0.7 and 0.3 MPa, respectively) were observed in samples milled for 10 h, corresponding to the formation and dissolution of βTiFeH phase. Different plateau pressures are related to the different amount of strain remained in the reacted samples. This observation is supported by results presented by Zaluski *et al.* [26] and Abe *et al.* [30]. According to them as the amount of strain in the as-milled samples is reduced (in those case, by different annealing temperature or time), the plateau pressures is increased, meaning more difficult hydrogenation. However, these sample also shown the lowest reversible storage capacity, only 0.522 wt.%, and a maximum storage capacity of 0.755 wt.% at 1.1 MPa. In this sense, better results were observed in samples milled for longer times (25 and 40 h), either for reversible or maximum capacity, e.g. 0.73 and 0.94 wt.%, respectively, at 1.9 MPa (40 h). The higher storage capacity attained at these samples can be explained by the higher amount of the TiFe phase (≥98 wt.% to samples milled for longer times, Table 2), as well as a better reversibility of the first absorbed hydrogen. In fact, post-hydrogenation analysis (by inert gas fusion-infrared absorptiometry) indicated that part of hydrogen absorbed by the first time became trapped, mainly in sample milled for 10 h (up to 0.15 wt.% could not be reversed), which justify the lowest reversible and maximum capacities. This sample has lower reversible capacity than samples milled for 25 and 40 h, since the TiFe formation is also lower. But samples milled for 5 h has even less TiFe and higher reversible capacity than sample milled for 10 h. It seems to be related to the mean crystallite size decrease and microstrain increase observed in that sample (10 h). It could be explained by hydrogen atoms trapping in crystal defects as suggested before by Hotta *et al.* [29].

It should be emphasized that after the reaction, 10 h milled sample showed the lower mean crystallite size and the higher microstrain compared to others, as seen if Fig. 7. Before reaction, in the as-milled condition, samples milled for 25 and 40 h showed indeed even higher degree of crystalline defects and strain, as can be seen in Fig. 2, since diffraction patterns exhibit larger broadening than that from 10 h milled sample (the mean crystallite size and microstrain were not possible to be determined in those cases by the Rietveld method). Mean crystallite size of the reacted samples milled for 25 and 40 h

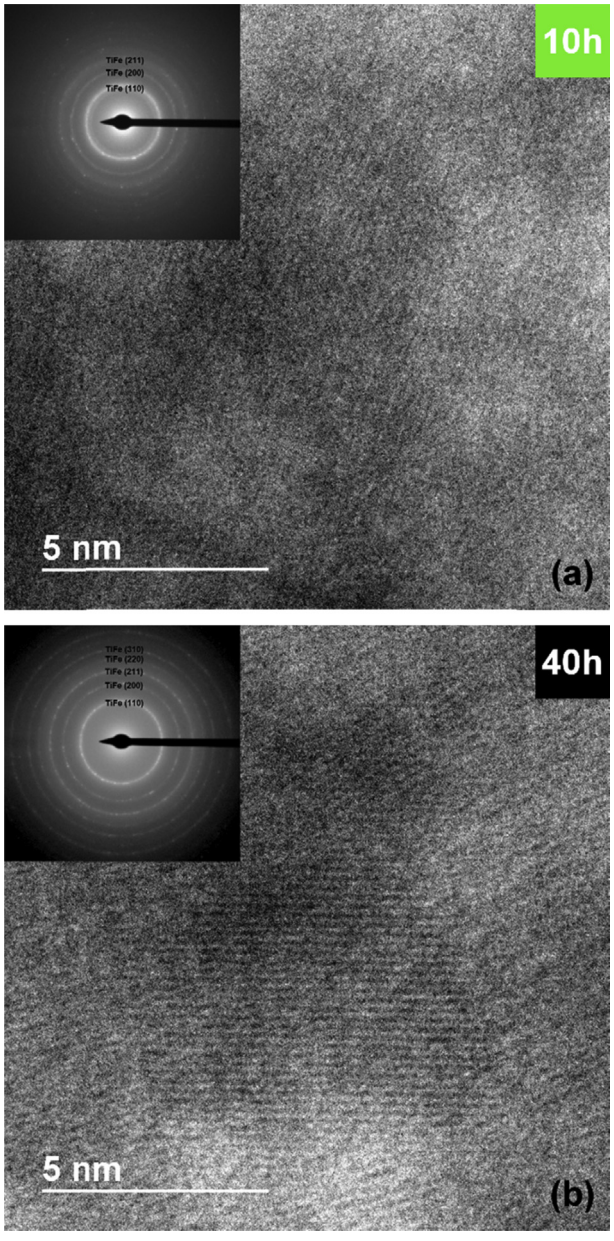

Fig. 8 – TEM images of the TiFe reacted samples previously milled for (a) 10 h and (b) 40 h.

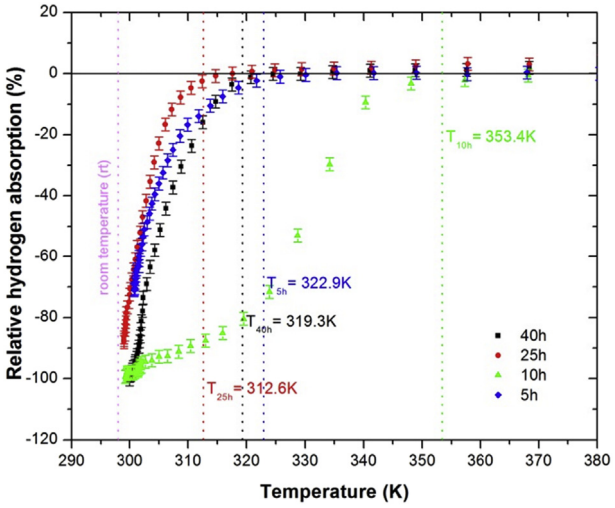

Fig. 9 – First hydrogen absorption during the reacted TiFe cooling process.

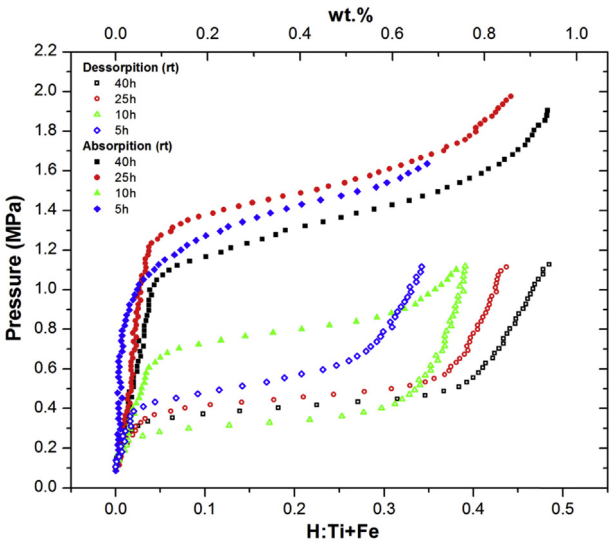

Fig. 10 – P-C isotherms (at room temperature) of reacted TiFe.

are very close compared to those from 10 h milled sample. However, the microstrain of the reacted 10 h milled samples is significantly higher, probably due to the chemical heterogeneity verified in that sample and commented before, which will be further investigated in a next publication.

As for the sorption kinetics of TiFe samples, it was verified that desorption flow rates are always higher than absorption flow rates, regardless of the milling time (see Fig. 11). Besides, the flow rates measured during the hydride formation (α+β phase field) are higher than others (α and β). The highest flow rates for both absorption (1.3 $cm^3 . min^{-1} . g^{-1}$) and desorption (2.0 $cm^3 . min^{-1} . g^{-1}$) were attained by TiFe samples from 10 h milling (increase up to 84 and 96% over to the worst absorption and desorption flow rates, respectively). This result corroborates the fact that this sample is more easily hydrogenated as observed previously in the first hydrogen absorption section.

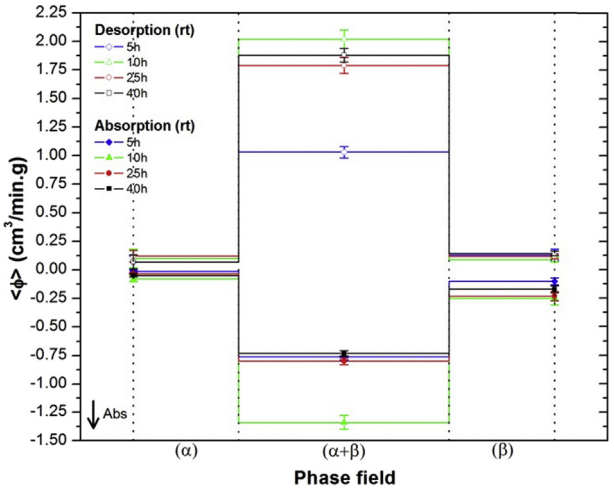

Fig. 11 – Average hydrogen flow rates (<ϕ>) measured during hydrogen sorption on TiFe samples (phase fields are indicated).

Conclusion

TiFe compound was successfully produced by the investigated process route, in which Ti was replaced by TiH_2 in milling with Fe. First, milling operation was accomplished well, with yields ranging from 90 to 95 wt.%. In turn, the reaction gain for the compound synthesis were higher than 98 wt.% (for 25 and 40 h of milling). The compound produced by this way (by post-heating milled samples at 873 K under vacuum) is nanocrystalline (13–21 nm), despite the elevated reaction temperature, and can be hydrogenated *in situ* during its cooling to the room temperature, requiring no thermal activation cycles (active compound). The compound that comes from samples milled for 10 h was more easily hydrogenated, since it could be able to absorb hydrogen before the others on cooling (at higher temperature) and has the lowest plateau pressures in P–C isotherms (0.7 MPa). Concerning easy hydrogenation, this superior behavior was attributed to a change in the stoichiometry of the compound (Ti-rich), occurred from some heterogeneity during milling TiH_2 and Fe powder mixture for shorter times (5 and 10 h). Higher reversible and storage capacities were shown however by samples milled for longer times (25 and 40 h), since TiFe phase content is higher and less hydrogen was trapped after the first hydrogen absorption in these samples as well. Work is currently being under way for processing non-stoichiometric TiFe by purpose, aiming to obtain better hydrogen sorption properties.

Acknowledgements

This work was financially supported by São Paulo Research Foundation (FAPESP, grants #2001/03961–4 and #2007/50018–2) and National Counsil for Technological and Scientific Development (CNPq, grants #481079/2008-4 and #482023/2011-2). R. B. Falcão acknowledges National Counsil for Technological and Scientific Development (CNPq) and Nuclear and Energy Research Institute (IPEN/CNEN-SP) for research fellowships and technical support, respectively.

REFERENCES

[1] Reilly JJ, Wiswall RH. Formation and properties of iron titanium hydride. Inorg Chem 1974;13:218–22. https://doi.org/10.1021/ic50131a042.

[2] Sakintuna B, Lamari-Darkrim F, Hirscher M. Metal hydride materials for solid hydrogen storage: a review. Int J Hydrogen Energy 2007;32:1121–40. https://doi.org/10.1016/j.ijhydene.2006.11.022.

[3] Schlapbach L, Züttel A. Hydrogen-storage materials for mobile applications. Nature 2001;414:353–8. https://doi.org/10.1038/35104634.

[4] Hoffman K, Reilly J, Salzano C, Waide R, Winsche W. Metal hydride storage for mobile and stationay applications. Int J Hydrogen Energy 1976;I:133–51.

[5] Endo N, Suzuki S, Goshome K, Maeda T. Operation of a bench-scale TiFe-based alloy tank under mild conditions for low-cost stationary hydrogen storage. Int J Hydrogen Energy

,0,0,42:5246–51. https://doi.org/10.1016/j.ijhydene.2016.11.088.
[6] Fiori C, Dell'Era A, Zuccari F, Santiangeli A, D'Orazio A, Orecchini F. Hydrides for submarine applications: overview and identification of optimal alloys for air independent propulsion maximization. Int J Hydrogen Energy 2015;40:11879–89. https://doi.org/10.1016/j.ijhydene.2015.02.105.
[7] Schlapbach L, Riesterer T. The activation of FeTi for hydrogen absorption. Appl Phys A Solids Surfaces 1983;32:169–82. https://doi.org/10.1007/BF00820257.
[8] Kim HC, Lee J. A study on the activation mechanism of FeTi in view of surface conditions of metals. Int J Hydrogen Energy 1985;10:543–5. https://doi.org/10.1016/0360-3199(85)90085-0.
[9] Ma J, Pan H, Wang X, Chen C, Wang Q. Hydrogen storage properties of FeTi1.3+x wt%Mm (x=0.0, 1.5, 3.0, 4.5, 6.0) hydrogen storage alloys. Int J Hydrogen Energy 2000;25:779–82. https://doi.org/10.1016/S0360-3199(99)00100-7.
[10] Ali W, Hao Z, Li Z, Chen G, Wu Z, Lu X, et al. Effects of Cu and Y substitution on hydrogen storage performance of TiFe0.86Mn0.1Y0.1–xCux. Int J Hydrogen Energy 2017;42:16620–31. https://doi.org/10.1016/j.ijhydene.2017.04.247.
[11] Lee SM, Perng TP. Correlation of substitutional solid solution with hydrogenation properties of TiFe1-xMx (M = Ni, Co, Al) alloys. J Alloy Comp 1999;291:254–61. https://doi.org/10.1016/S0925-8388(99)00262-5.
[12] Boulghallat M, Gerard N. Hydriding kinetics of TiFe0.5Co0.5 compounds. J Less Common Met 1991;172–174:1052–7. https://doi.org/10.1016/S0022-5088(06)80011-1.
[13] Lee S-M, Perng T-P. Effect of the second phase on the initiation of hydrogenation of TiFe1–xMx (M = Cr,Mn) alloys☆. Int J Hydrogen Energy 1994;19:259–63. https://doi.org/10.1016/0360-3199(94)90095-7.
[14] Chung HS, Lee JY. Effect of partial substitution of Mn and Ni for Fe in FeTi on hydriding kinetics. Int J Hydrogen Energy 1986;11:335–9. https://doi.org/10.1016/0360-3199(86)90153-9.
[15] Fukushima S, Tanabe H. Surface properties of TiFe and TiFe-Nb 6.8 at.% electrodes in aqueous solution. Int J Hydrogen Energy 1983;8:33–7. https://doi.org/10.1016/0360-3199(83)90032-0.
[16] Sasai T, Oku K, Konno H, Onouwe K, Kashu S. Hydrogen storage characteristics of Fe-Ti-Zr-Nb alloys. J Less-Common Met 1983;89:281–5. https://doi.org/10.1016/0022-5088(83)90281-3.
[17] Nagai H, Nakatsu M, Shoji K, Tamura H. Effect of simultaneous addition of oxygen with copper or niobium on the hydriding characteristics of FeTi for hydrogen storage. J Less-Common Met 1986;119:131–42. https://doi.org/10.1016/0022-5088(86)90203-1.
[18] Singh BK, Singh AK, Srivastava ON. On the synthesis, characterization and hydrogenation behaviour of Fe1 $minus; xTi1 + yNix (x = 0.2, Y = 0.3) hydrogen storage material. Int J Hydrogen Energy 1997;22:805–8. https://doi.org/10.1016/S0360-3199(96)00218-2.
[19] Kulshreshtha SK, Jayakumar OD, Bhatt KB. Hydriding characteristics of palladium and platinum alloyed FeTi. J Mater Sci 1993;28:4229–33. https://doi.org/10.1007/BF00351259.
[20] Yamashita I, Tanaka H, Takeshita H, Kuriyama N, Sakai T, Uehara I. Hydrogenation characteristics of TiFe1–xPdx (0.05≤x≤0.30) alloys. J Alloy Comp 1997;253–254:238–40. https://doi.org/10.1016/S0925-8388(96)02925-8.
[21] Qu H, Du J, Pu C, Niu Y, Huang T, Li Z, et al. Effects of Co introduction on hydrogen storage properties of Ti-Fe-Mn alloys. Int J Hydrogen Energy 2015;40:2729–35. https://doi.org/10.1016/j.ijhydene.2014.12.089.
[22] Rajalakshmi N, Dhathathereyan K. Hydrogen solubility properties of Ti0.42Zr0.08Fe0.50 alloy. Int J Hydrogen Energy 1999;24:625–9. https://doi.org/10.1016/S0360-3199(98)00121-9.
[23] Lv P, Huot J. Hydrogen storage properties of Ti0.95FeZr0.05, TiFe0.95Zr0.05 and TiFeZr0.05 alloys. Int J Hydrogen Energy 2016;41:22128–33. https://doi.org/10.1016/j.ijhydene.2016.07.091.
[24] Patel AK, Sharma P, Huot J. Effect of annealing on microstructure and hydrogenation properties of TiFe + X wt % Zr (X = 4, 8). Int J Hydrogen Energy 2018;43:6238–43. https://doi.org/10.1016/j.ijhydene.2018.02.029.
[25] Ali W, Li M, Gao P, Wu C, Li Q, Lu X, et al. Hydrogenation properties of Ti-Fe-Mn alloy with Cu and Y as additives. Int J Hydrogen Energy 2017;42:2229–38. https://doi.org/10.1016/j.ijhydene.2016.09.037.
[26] Zaluski L, Tessier P, Ryan DH, Doner CB, Zaluska A, Ström-Olsen JO, et al. Amorphous and nanocrystalline Fe-Ti prepared by ball milling. J Mater Res 1993;8:3059–68. https://doi.org/10.1557/JMR.1993.3059.
[27] Jung CB, Kim JH, Lee KS. Electrode characteristics of nanostructured TiFe and ZrCr2 type metal hydride prepared by mechanical alloying. Nanostruct Mater 1997;8:1093–104. https://doi.org/10.1016/S0965-9773(98)00033-6.
[28] Novakova AA, Agladze OV, Tarasov BP. Structure tranformations during mechanical griding of Fe-TiH_2 mixture. Russ J Inorg Chem 2000;45:1168–72.
[29] Hotta H, Abe M, Kuji T, Uchida H. Synthesis of Ti-Fe alloys by mechanical alloying. J Alloy Comp 2007;439:221–6. https://doi.org/10.1016/j.jallcom.2006.05.137.
[30] Abe M, Kuji T. Hydrogen absorption of TiFe alloy synthesized by ball milling and post-annealing. J Alloy Comp 2007;446–447:200–3. https://doi.org/10.1016/j.jallcom.2006.12.063.
[31] Haraki T, Oishi K, Uchida H, Miyamoto Y, Abe M, Kokaji T, et al. Properties of hydrogen absorption by nano-structured FeTi alloys. Int J Mater Res 2008;99:507–12. https://doi.org/10.3139/146.101669.
[32] Abrashev B, Spassov T, Bliznakov S, Popov A. Microstructure and electrochemical hydriding/dehydriding properties of ball-milled TiFe-based alloys. Int J Hydrogen Energy 2010;35:6332–7. https://doi.org/10.1016/j.ijhydene.2010.03.129.
[33] Zadorozhnyy V, Klyamkin S, Zadorozhnyy M, Bermesheva O, Kaloshkin S. Hydrogen storage nanocrystalline TiFe intermetallic compound: synthesis by mechanical alloying and compacting. Int J Hydrogen Energy 2012;37:17131–6. https://doi.org/10.1016/j.ijhydene.2012.08.078.
[34] Zadorozhnyy VY, Milovzorov GS, Klyamkin SN, Zadorozhnyy MY, Strugova DV, Gorshenkov MV, et al. Preparation and hydrogen storage properties of nanocrystalline TiFe synthesized by mechanical alloying. Prog Nat Sci Mater Int 2017;27:149–55. https://doi.org/10.1016/j.pnsc.2016.12.008.
[35] Aoyagi H, Aoki K, Masumoto T. Effect of ball milling on hydrogen absorption properties of FeTi, Mg2Ni and LaNi5. J Alloy Comp 1995;231:804–9. https://doi.org/10.1016/0925-8388(95)01721-6.
[36] Bououdina M, Fruchart D, Jacquet S, Pontonnier L, Soubeyroux JL. Effect of nickel alloying by using ball milling on the hydrogen absorption properties of TiFe. Int J Hydrogen Energy 1999;24:885–90. https://doi.org/10.1016/S0360-3199(98)00163-3.
[37] Chiang CH, Chin ZH, Perng TP. Hydrogenation of TiFe by high-energy ball milling. J Alloy Comp 2000;307:259–65. https://doi.org/10.1016/S0925-8388(00)00827-6.
[38] Davids MW, Lototskyy M. Influence of oxygen introduced in TiFe-based hydride forming alloy on its morphology,

structural and hydrogen sorption properties. Int J Hydrogen Energy 2012;37:18155–62. https://doi.org/10.1016/j.ijhydene.2012.09.106.

[39] Emami H, Edalati K, Matsuda J, Akiba E, Horita Z. Hydrogen storage performance of TiFe after processing by ball milling. Acta Mater 2015;88. https://doi.org/10.1016/j.actamat.2014.12.052.

[40] Zadorozhnyy VY, Klyamkin SN, Kaloshkin SD, Zadorozhnyy MY, Bermesheva OV. Mechanochemical synthesis and hydrogen sorption properties of nanocrystalline TiFe. Inorg Mater 2011;47:1081–6. https://doi.org/10.1134/S0020168511100232.

[41] Sandrock GD, Goodell PD. Surface poisoning of LaNi5, FeTi and (Fe,Mn)Ti by O2, CO and H2O. J Less-Common Met 1980;73:161–8. https://doi.org/10.1016/0022-5088(80)90355-0.

[42] Mizuno T, Morozumi T. Titanium concentration in FeTix ($1 \leq x \leq 2$) alloys and its effect on hydrogen storage properties. J Less Common Met 1982;84:237–44. https://doi.org/10.1016/0022-5088(82)90148-5.

[43] Lee SM, Perng TP. Microstructural correlations with the hydrogenation kinetics of FeTi1+x alloys. J Alloy Comp 1991;177:107–18. https://doi.org/10.1016/0925-8388(91)90061-Y.

[44] Falcão RB, Dammann EDCC, Rocha CJ, Leal Neto RM. An investigation on the mechanical alloying of TiFe compound by high-energy ball milling. Mater Sci Forum 2010;661:329–34. https://doi.org/10.4028/www.scientific.net/MSF.660-661.329.

[45] Falcão RB, Dammann EDCC, da Rocha CJ, Ichikawa RU, Durazzo M, Martinez LG. Leal neto RM. Synthesis of TiFe compound from ball milled TiH_2 and Fe powders mixtures. Mater Sci Forum 2014;802:61–5. https://doi.org/10.4028/www.scientific.net/MSF.802.61.

[46] Balzar D. Voigt-function model in diffraction line-broadening analysis. Microstruct Anal from Diffr 1999;44. doi:10.1.1.30.7311.

[47] Abrahamson II EP, Lopata SL. Lattice parameters and solubility limits of alpha iron as affected by some binary transition-element additions. Trans Metall Soc AIME 1966;236:76–87.

[48] Suryanarayana C. Mechanical alloying and milling. Prog Mater Sci 2001;46:1–184. https://doi.org/10.1016/S0079-6425(99)00010-9.

[49] Murty BS, Ranganathan S. Novel materials synthesis by mechanical alloying/milling. Int Mater Rev 1998;43:101–41. https://doi.org/10.1179/095066098790105654.